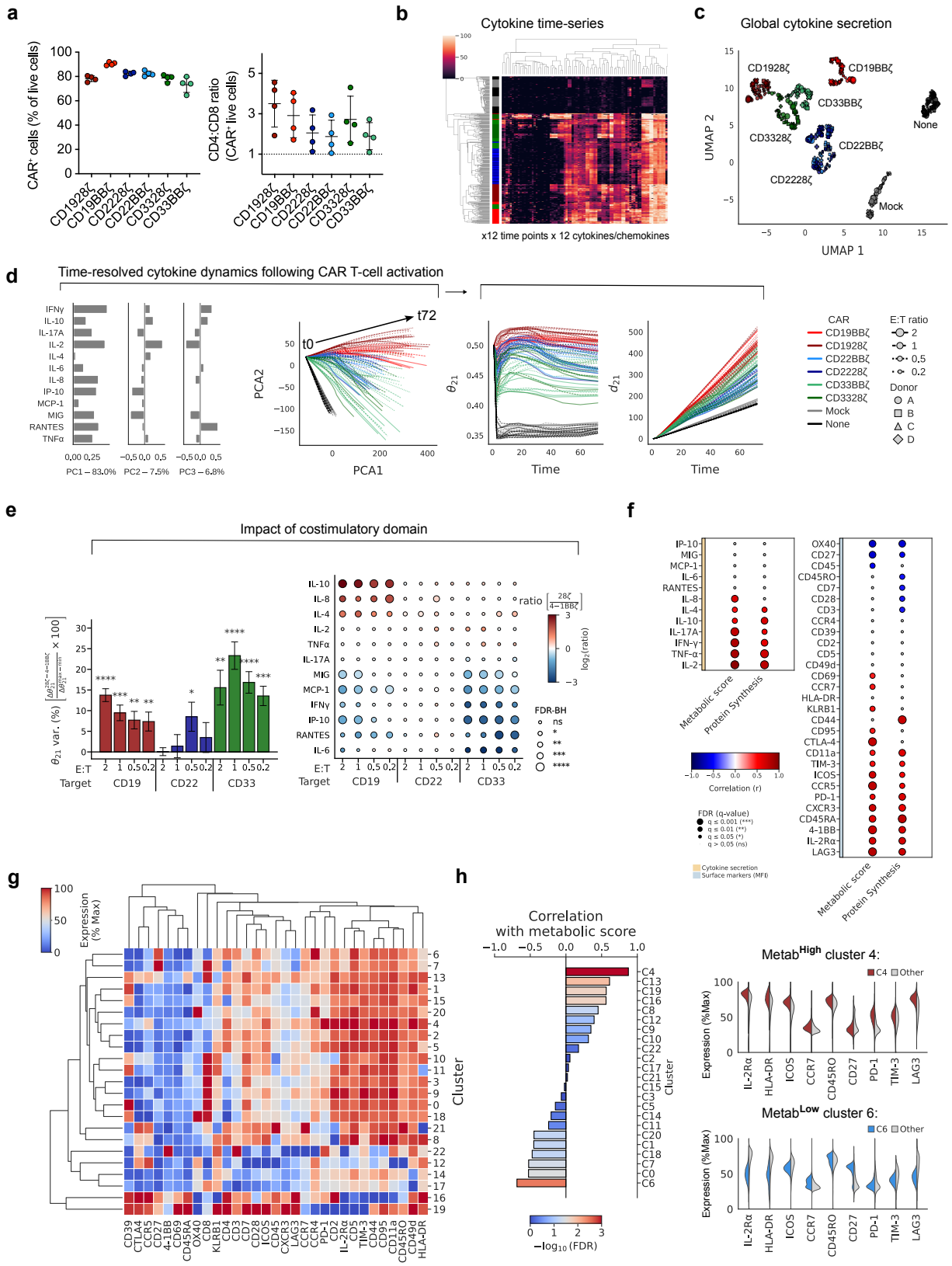
a
CAR+ cells (% of live cells)
CD4:CD8 ratio (CAR+ live cells)
CD1928ζ
CD19BBζ
CD2228ζ
CD22BBζ
CD3328ζ
CD33BBζ
b
Cytokine time-series
x12 time points x 12 cytokines/chemokines
c
Global cytokine secretion
UMAP 1
UMAP 2
None
Mock
d
Time-resolved cytokine dynamics following CAR T-cell activation
IFNγ
IL-10
IL-17A
IL-2
IL-4
IL-6
IL-8
IP-10
MCP-1
MIG
RANTES
TNFα
PC1 – 83.0%
PC2 – 7.5%
PC3 – 6.8%
t0
t72
PCA1
PCA2
Time
CAR
E:T ratio
Donor
e
Impact of costimulatory domain
Target
CD19
CD22
CD33
FDR-BH
f
Metabolic score
Protein Synthesis
Correlation (r)
FDR (q-value)
Cytokine secretion
Surface markers (MFI)
g
Expression (% Max)
Cluster
h
Correlation with metabolic score
−log10 (FDR)
Metab^High cluster 4:
Metab^Low cluster 6:
C4
Other
C6

Extended Data Figure 1. Immuno-metabolic profiling framework and extended characterization of CAR T-cell states

a, CAR transduction efficiency and CD4:CD8 ratios across CAR T-cell constructs and donors.

b, Hierarchical clustering of all cytokine and chemokine measurements across experimental conditions is shown (right). Each row represents a unique CAR construct × donor × E:T ratio condition, and each column represents one of 12 cytokines/chemokines measured at 12 time points over 72 h. (n = 4 biological replicates)

c, UMAP projection of cytokine secretion profiles. Each point represents the integral of log-transformed levels of 12 cytokines and chemokines across a 72-h time course for a given condition. Colors, symbol shapes, and symbol sizes represent CAR construct, donor, and effector-to-target (E:T) ratio, respectively.

d, Quantification of cytokine secretion trajectories. Cumulative integrals of log10-transformed cytokine concentrations were computed at each time point and projected into principal component space (left). Trajectory angle (θ_{21}) and radial distance (d21) were derived over time (middle) and summarized as median trajectory angle relative to trajectory speed (v21) (right).

e, Effects of CD28ζ and 4-1BBζ costimulatory domains on cytokine trajectory dynamics (left) and secretion of individual cytokines (right).

f, Comparative associations of composite metabolic activity score and protein synthesis with individual cytokines and phenotypic markers.

g, Hierarchical clustering of spectral flow cytometry-defined CAR T-cell populations identified using the PARC algorithm.

h, Associations between CAR T-cell cluster frequencies and composite metabolic activity score. Representative marker expression profiles of metabolically high ($Metab^{High}$) and metabolically low ($Metab^{Low}$) CAR T-cell clusters are shown.

Statistical significance was determined using two-tailed one-sample Student's *t*-tests (e) or Pearson correlation analysis with Benjamini–Hochberg correction for multiple comparisons (f, h). *P* values are indicated as follows: $^{*}P < 0.05$, $^{**}P < 0.01$, $^{***}P < 0.001$, and $^{****}P < 0.0001$; ns, not significant.

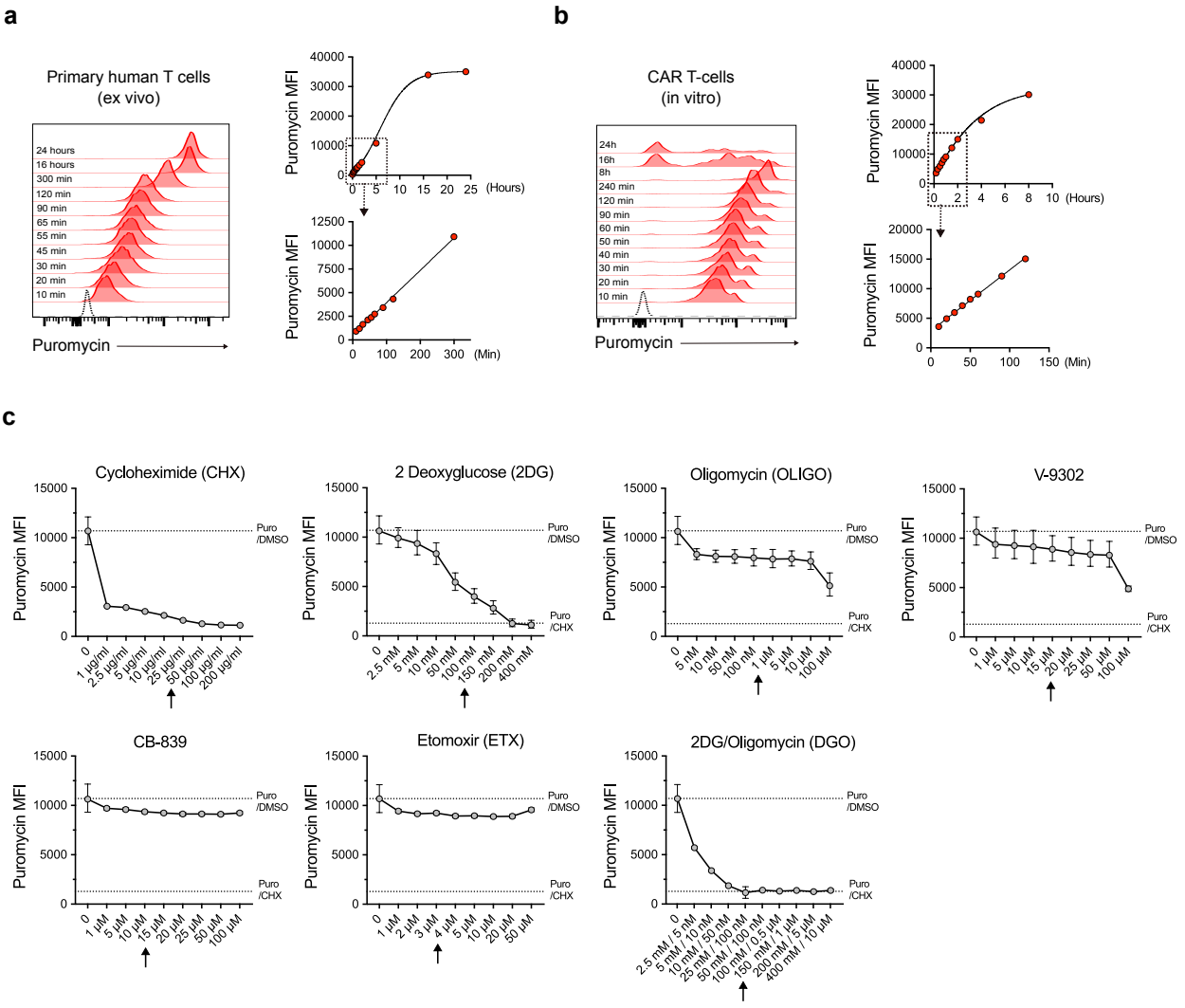
a
Primary human T cells
(ex vivo)
24 hours
16 hours
300 min
120 min
90 min
65 min
55 min
45 min
30 min
20 min
10 min
Puromycin
Puromycin MFI
(Hours)
(Min)
b
CAR T-cells
(in vitro)
24h
16h
8h
240 min
120 min
90 min
60 min
50 min
40 min
30 min
20 min
10 min
Puromycin
Puromycin MFI
(Hours)
(Min)
c
Cycloheximide (CHX)
2 Deoxyglucose (2DG)
Oligomycin (OLIGO)
V-9302
CB-839
Etomoxir (ETX)
2DG/Oligomycin (DGO)
Puromycin MFI
Puro /DMSO
Puro /CHX

Extended Data Figure 2. Optimization of puromycin incorporation kinetics and metabolic perturbation assays.

a–b, Time course of puromycin incorporation in activated primary human T-cells (a) and CAR T-cells (b). Representative histograms and quantification of puromycin mean fluorescence intensity (MFI) are shown. Upper panels depict the full incorporation time course, whereas lower panels highlight the initial linear phase of puromycin incorporation.

c, Dose-response effects of metabolic and translational inhibitors on puromycin incorporation in CAR T cells expanded in vitro. Cells were treated with cycloheximide (CHX), 2-deoxyglucose (2DG), oligomycin (OLIGO), V-9302, CB-839, etomoxir (ETX), or combined 2DG/oligomycin (DGO) at the indicated concentrations for 15 minutes prior to puromycin incorporation and intracellular anti-puromycin staining. Arrows indicate concentrations used in subsequent experiments.

a

Target	Tbet	LiveDead	CD62L	CD25	CCR7	CXCR3	CD28	CD69	CCR4	CD127	CD45RO	PD1	CD45RA	ICOS	TIM3	CCR5
Fluorochrome	BUV395	Fixable Blue	BUV496	BUV563	BUV615	BUV661	BUV737	BUV805	BV421	Pacific Blue	BV570	BV605	BV650	BV711	BV750	BV785
Target	Puromycin	CD95	CD71	TCF1	CD8	4-1BB	CD3	LAG3	HELIOS	*CAR*	CD4	CD39	CD27			
Fluorochrome	Alexa Fluor 488	BB700	RB780	PE	Spark YG 593	PE-Dazzle 594	PE-Cy5	PE-Fire 700	PE-Cy7	Alexa Fluor 647	Alexa Fluor 700	APC-Cy7	APC-Fire 810			

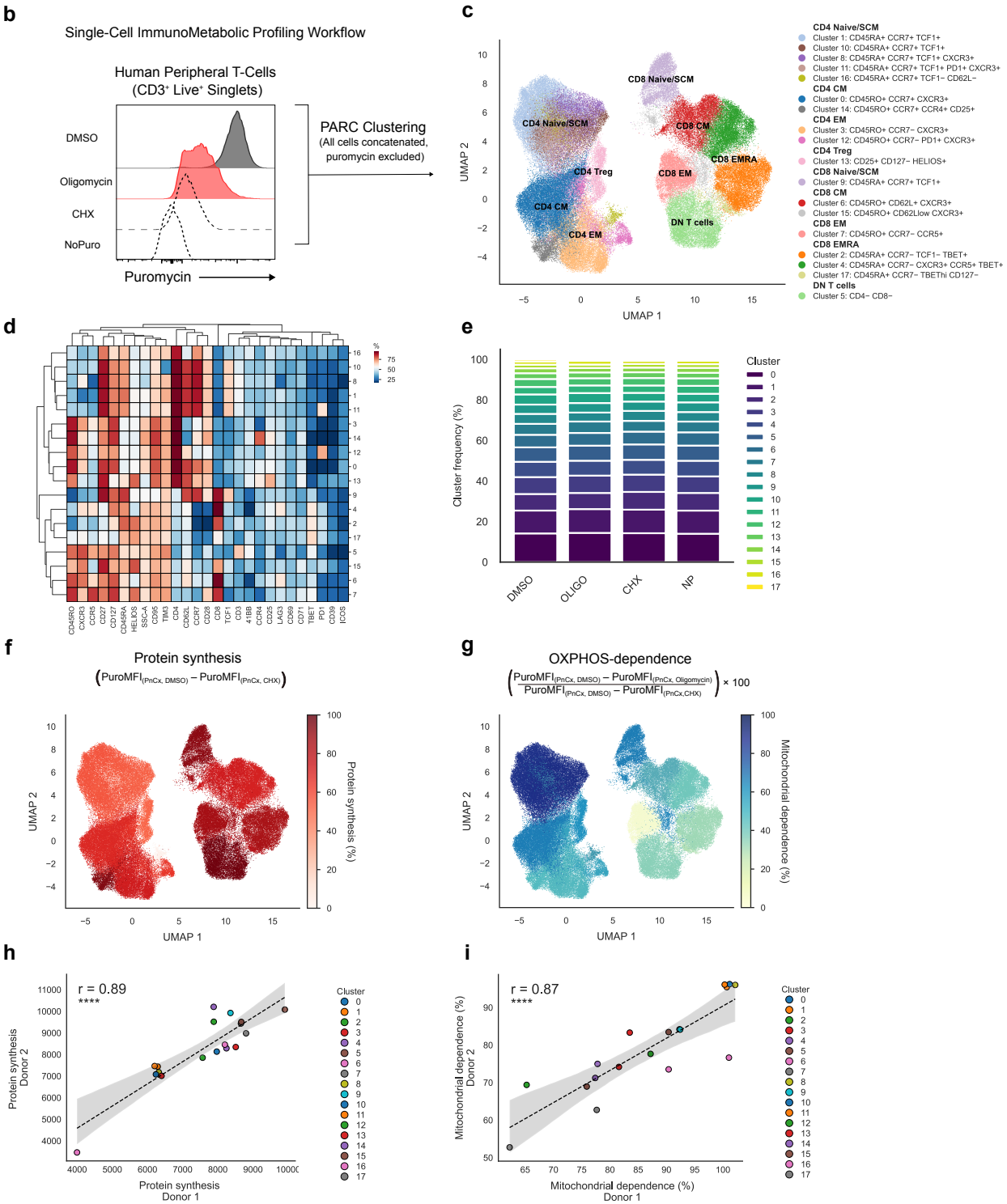

Extended Data Figure 3. Single-cell immuno-metabolic profiling using puromycin-based protein synthesis assays.

a, Spectral flow cytometry panel used for puromycin-based single-cell immuno-metabolic profiling, with CAR detection reagent highlighted in gray.

b–g, Validation of a spectral flow cytometry–based single-cell immuno-metabolic profiling workflow.

b, Representative histograms showing puromycin incorporation in ex vivo peripheral blood T-cells from healthy donors under DMSO, oligomycin, cycloheximide (CHX), and no-puromycin conditions.

c–d, PARC clustering of all ex vivo human peripheral blood T-cells pooled across DMSO-, oligomycin-, cycloheximide (CHX)-, and no-puromycin conditions. Clustering was performed using only phenotypic markers, with puromycin excluded from clustering analyses. (c) UMAP visualization of PARC-defined T-cell clusters. (d) Hierarchical clustering heatmap showing phenotypic marker expression across PARC-defined clusters.

e, Relative abundance of PARC-defined T-cell clusters across DMSO-, oligomycin-, cycloheximide (CHX)-, and no-puromycin–treated conditions.

f–g, UMAP visualization of *ex vivo* peripheral blood T-cells colored according to protein synthesis (left) or OXPHOS dependence (right). Protein synthesis was quantified by puromycin incorporation relative to cycloheximide-treated controls, whereas OXPHOS dependence was calculated from the reduction in puromycin incorporation following oligomycin treatment.

h–i, Correlation of protein synthesis (h) and OXPHOS dependence (i) measurements across PARC-defined T-cell clusters between independent healthy donors.

Statistical significance was determined using Pearson correlation analysis (h–i). *P* values are indicated as follows: $^{*}P < 0.05$, $^{**}P < 0.01$, $^{***}P < 0.001$, and $^{****}P < 0.0001$; ns, not significant.

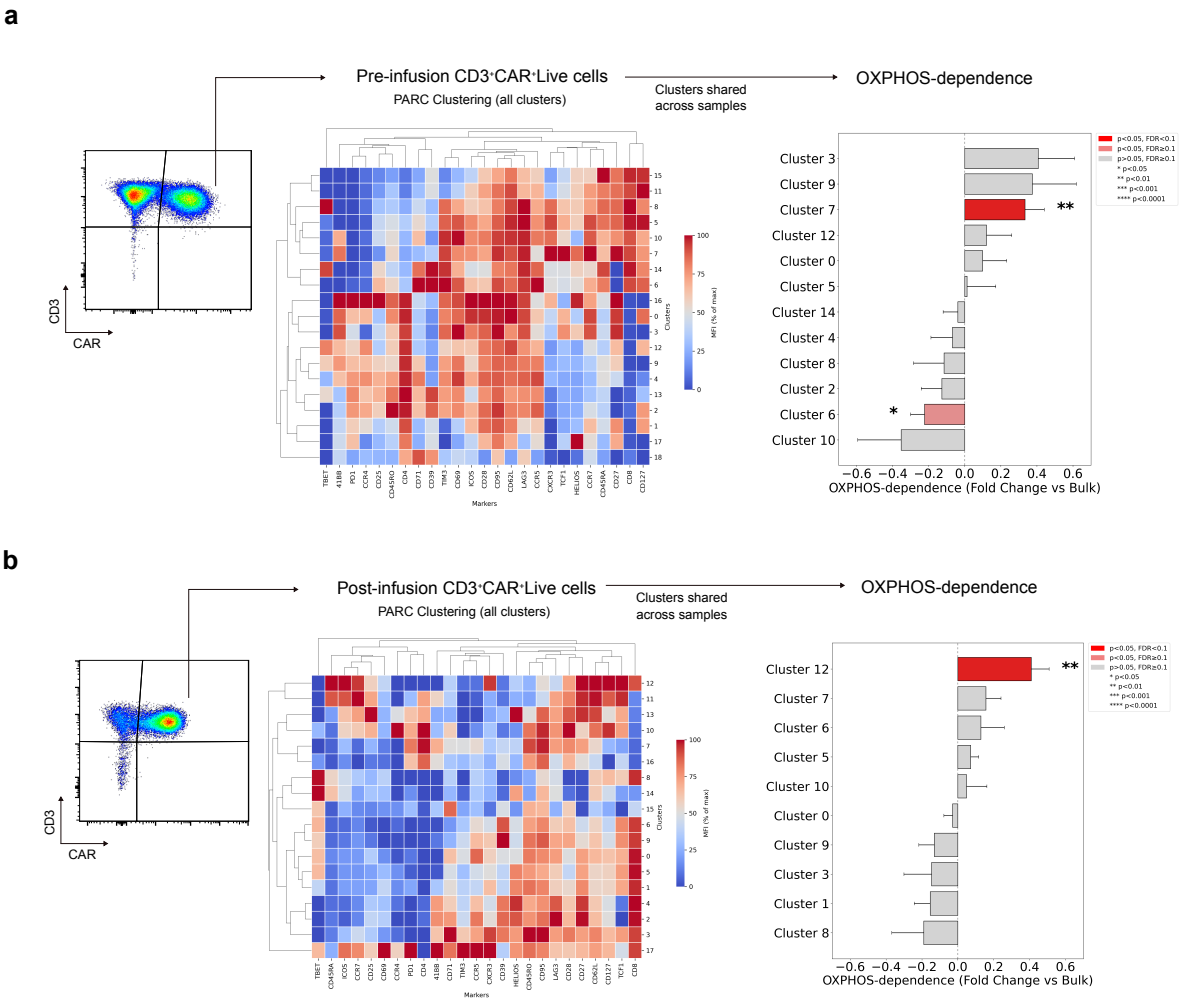
a
Pre-infusion CD3+CAR+Live cells
PARC Clustering (all clusters)
Clusters shared across samples
OXPHOS-dependence
CD3
CAR
Markers
Clusters
MFI (% of max)
Cluster 3
Cluster 9
Cluster 7
Cluster 12
Cluster 0
Cluster 5
Cluster 14
Cluster 4
Cluster 8
Cluster 2
Cluster 6
Cluster 10
OXPHOS-dependence (Fold Change vs Bulk)
b
Post-infusion CD3+CAR+Live cells
PARC Clustering (all clusters)
Clusters shared across samples
OXPHOS-dependence
Cluster 12
Cluster 7
Cluster 6
Cluster 5
Cluster 10
Cluster 0
Cluster 9
Cluster 3
Cluster 1
Cluster 8
OXPHOS-dependence (Fold Change vs Bulk)
c
Post-infusion Cluster8:
CD8+CD28-CD27-TCF1low
Cluster 8 (%)
CR
No CR
Expression (% Max)
CD8
CD28
CD27
TCF1

Extended Data Figure 4. Single-cell metabolic profiling of pre- and post-infusion CAR T-cell subsets.

a–b, Single-cell metabolic profiling of pre-infusion (a) and post-infusion (b) $CD3^{+}CAR^{+}$ T-cells from patients enrolled in the CD22 CAR T-cell trial. Representative gating strategy and hierarchical clustering heatmaps of PARC-defined clusters based on phenotypic marker expression (left and middle), together with relative OXPHOS dependence of individual clusters compared with the bulk CAR T-cell population (right), are shown. Only clusters shared across patients are presented.

c, Frequency and phenotypic characterization of post-infusion terminally differentiated Cluster C8 enriched in patients with no complete remission (No CR). Cluster frequencies in patients with complete remission (CR) and no complete remission (No CR) (left) and representative phenotypic marker expression profiles (right) are shown.

Statistical significance was determined using Wilcoxon signed-rank tests with Benjamini–Hochberg false discovery rate (FDR) correction (a–b) and Welch's two-sided unpaired *t*-tests (c). *P* values are indicated as follows: $^{*}P < 0.05$, $^{**}P < 0.01$, $^{***}P < 0.001$, and $^{****}P < 0.0001$; ns, not significant.

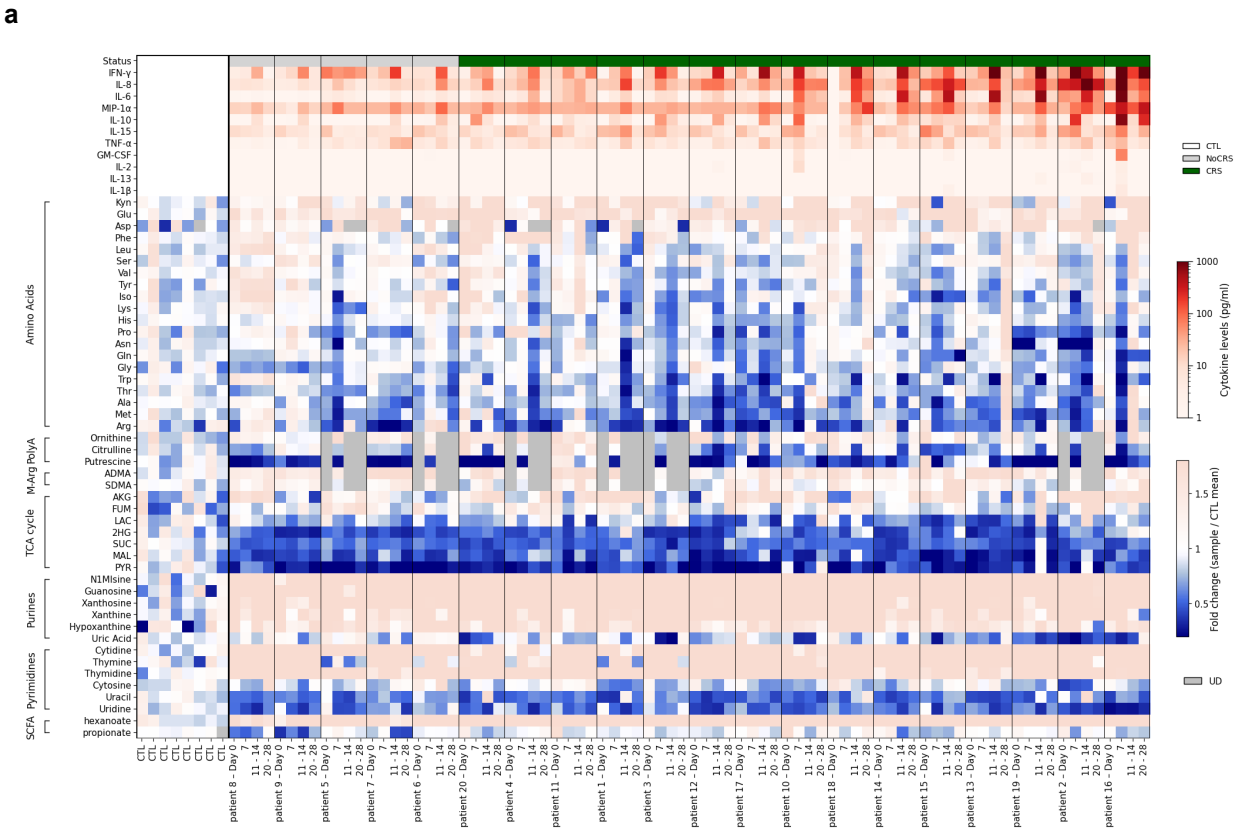
a
Status
IFN-γ
IL-8
IL-6
MIP-1α
IL-10
IL-15
TNF-α
GM-CSF
IL-2
IL-13
IL-1β
Kyn
Glu
Asp
Phe
Leu
Ser
Val
Tyr
Iso
Lys
His
Pro
Asn
Gln
Gly
Trp
Thr
Ala
Met
Arg
Ornithine
Citrulline
Putrescine
ADMA
SDMA
AKG
FUM
LAC
2HG
SUC
MAL
PYR
N1MIsine
Guanosine
Xanthosine
Xanthine
Hypoxanthine
Uric Acid
Cytidine
Thymine
Thymidine
Cytosine
Uracil
Uridine
hexanoate
propionate
Amino Acids
M-Arg PolyA
TCA cycle
Purines
Pyrimidines
SCFA
CTL
NoCRS
CRS
Cytokine levels (pg/ml)
Fold change (sample / CTL mean)
UD

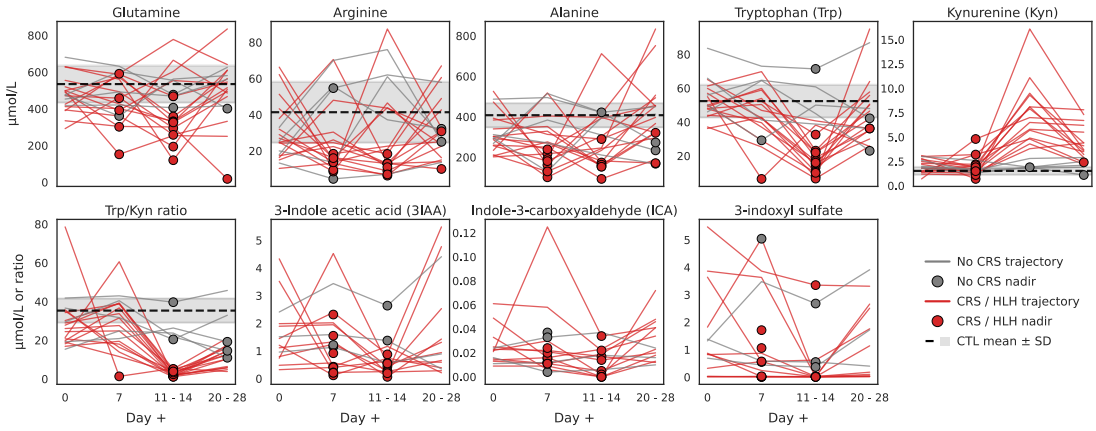
b
Glutamine
Arginine
Alanine
Tryptophan (Trp)
Kynurenine (Kyn)
Trp/Kyn ratio
3-Indole acetic acid (3IAA)
Indole-3-carboxyaldehyde (ICA)
3-indoxyl sulfate
µmol/L
µmol/L or ratio
Day +
No CRS trajectory
No CRS nadir
CRS / HLH trajectory
CRS / HLH nadir
CTL mean ± SD

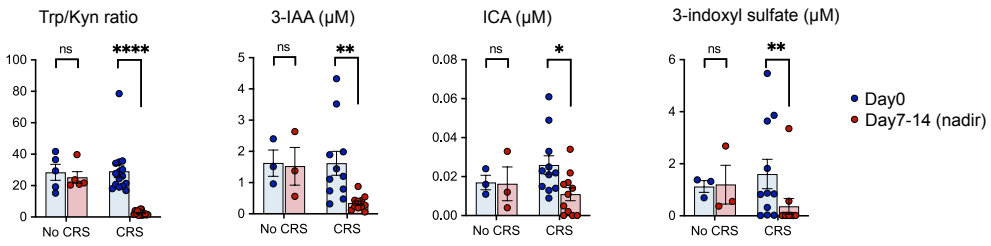
c
Trp/Kyn ratio
3-IAA (µM)
ICA (µM)
3-indoxyl sulfate (µM)
ns
****
**
*
No CRS
CRS
Day0
Day7-14 (nadir)

Extended Data Figure 5. Longitudinal plasma metabolomics during CAR T-cell expansion and cytokine release syndrome.

a, Longitudinal plasma metabolomics profiling of CAR T-cell–treated patients, ordered according to cytokine release syndrome (CRS) occurrence and circulating cytokine levels. Plasma cytokine levels (top) together with circulating metabolite levels, grouped by metabolic pathway and represented as fold change relative to healthy controls, are shown across patients and time points following CAR T-cell infusion.

b, Longitudinal plasma levels of selected amino acids and microbiota-derived metabolites in CAR T-cell–treated patients with or without cytokine release syndrome (CRS). Individual patient trajectories are shown across time points following infusion to demonstrate clinical kinetics.

c, Plasma levels of the tryptophan-to-kynurenine ratio (Trp/Kyn) and microbiota-derived tryptophan metabolites—including indole-3-carboxaldehyde (ICA), 3-indoxyl sulfate, and 3-indole acetic acid (3-IAA)—in CAR T-cell–treated patients with or without CRS at baseline and during the expansion phase following infusion.

Statistical significance was determined using two-tailed paired Student's *t*-tests (c). *P* values are indicated as follows: $^{*}P < 0.05$, $^{**}P < 0.01$, $^{***}P < 0.001$, and $^{****}P < 0.0001$; ns, not significant.

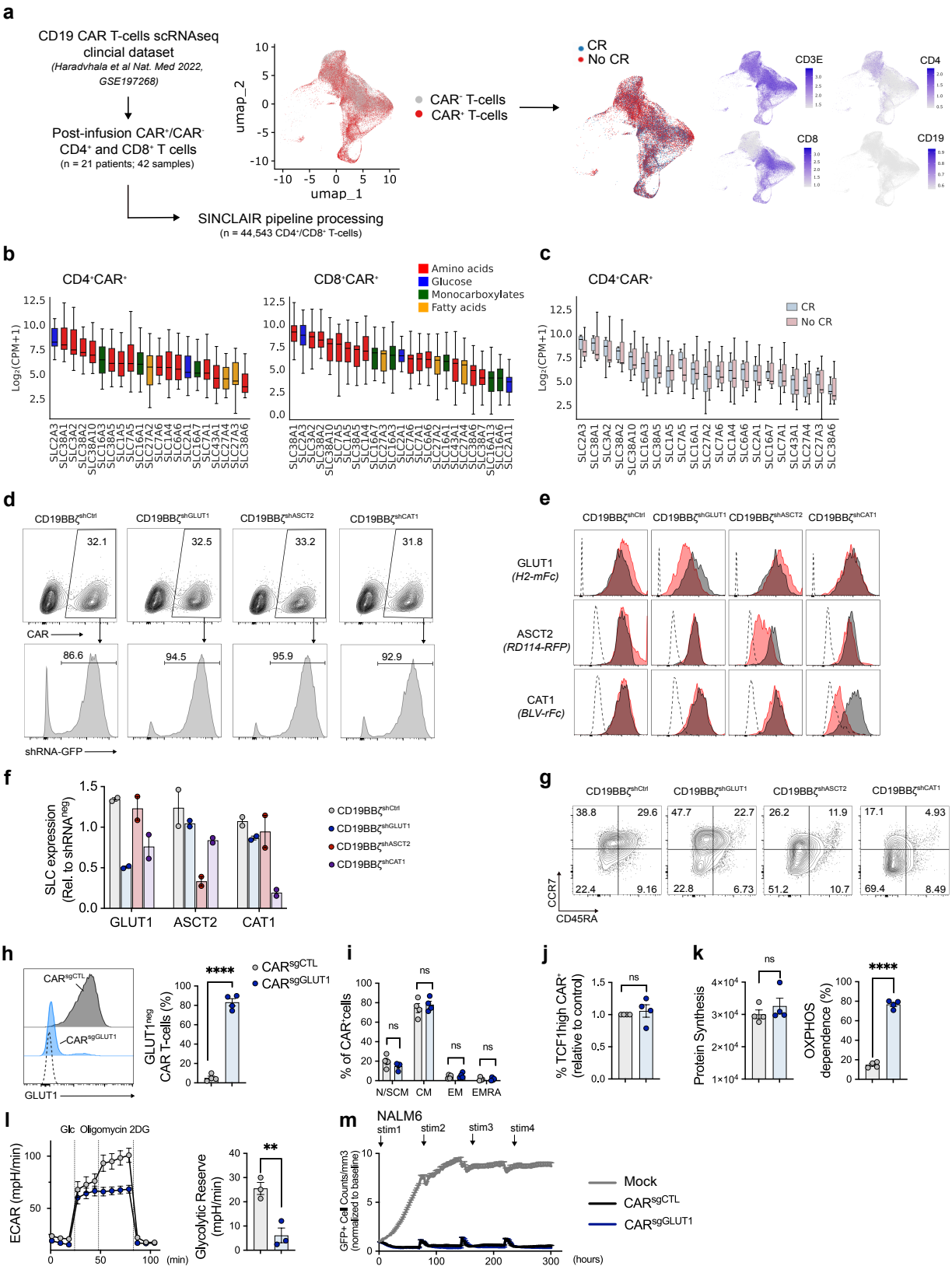
a
CD19 CAR T-cells scRNAseq clincial dataset
(Haradvhala et al Nat. Med 2022, GSE197268)
Post-infusion CAR+/CAR- CD4+ and CD8+ T cells
(n = 21 patients; 42 samples)
SINCLAIR pipeline processing
(n = 44,543 CD4+/CD8+ T-cells)
umap_1
umap_2
CAR- T-cells
CAR+ T-cells
CR
No CR
CD3E
CD4
CD8
CD19
b
CD4+CAR+
CD8+CAR+
Amino acids
Glucose
Monocarboxylates
Fatty acids
Log2(CPM+1)
c
CD4+CAR+
CR
No CR
d
CD19BBζshCtrl
CD19BBζshGLUT1
CD19BBζshASCT2
CD19BBζshCAT1
32.1
32.5
33.2
31.8
CAR
86.6
94.5
95.9
92.9
shRNA-GFP
e
GLUT1 (H2-mFc)
ASCT2 (RD114-RFP)
CAT1 (BLV-rFc)
f
SLC expression (Rel. to shRNAneg)
GLUT1
ASCT2
CAT1
g
38.8
29.6
47.7
22.7
26.2
11.9
17.1
4.93
22.4
9.16
22.8
6.73
51.2
10.7
69.4
8.49
CCR7
CD45RA
h
CARsgCTL
CARsgGLUT1
GLUT1
GLUT1neg CAR T-cells (%)
****
i
% of CAR+cells
ns
N/SCM
CM
EM
EMRA
j
% TCF1high CAR+ (relative to control)
k
Protein Synthesis
OXPHOS dependence (%)
l
Glc
Oligomycin
2DG
ECAR (mpH/min)
(min)
Glycolytic Reserve (mpH/min)
**
m
NALM6
stim1
stim2
stim3
stim4
GFP+ Cell Counts/mm3 (normalized to baseline)
(hours)
Mock
CARsgCTL
CARsgGLUT1

Extended Data Figure 6. Transcriptomic analysis of post-infusion patient CAR T-cells and functional characterization of SLC transporter modulation.

a, Analysis of publicly available post-infusion CD19 CAR T-cell scRNA-seq data from Haradhvala et al., Nat. Med. 2022. UMAP projections of CAR^+ and CAR^- T cells, complete responder (CR) and non-responder (No CR) samples, and representative lineage marker expression are shown.

b, Expression of detectable SLC transporter family members in post-infusion $CD4^+CAR^+$ and $CD8^+CAR^+$ T-cell subsets, shown as pseudo-bulk expression levels. SLCs are color-coded according to their transport of amino acids, glucose, monocarboxylate, and fatty acids.

c, Expression of detectable SLC transporter family members in post-infusion $CD4^+CAR^+$ T cells, stratified by clinical response: responders (CR, blue) and non-responders (No CR, red).

d, Representative flow cytometry plots showing CAR transduction efficiency and shRNA expression across CAR T-cell conditions targeting GLUT1, ASCT2, and CAT1.

e, Quantification of cell-surface expression of ASCT2, CAT1, and GLUT1 proteins by flow cytometry following shRNA-mediated knockdown relative to non-targeting controls (shCtrl).

f, Relative cell surface levels of GLUT1, ASCT2, and CAT1 across shRNA conditions measured by flow cytometry.

g, Representative flow cytometry plots showing the gating and distribution of naïve/stem cell memory (N/SCM), central memory (CM), effector memory (EM), and effector memory RA-positive (EMRA) CAR T-cells subsets following specific shRNA transporter modulation.

h, Flow cytometric validation (left) confirming complete knockout of GLUT1 protein expression in CRISPR/Cas9-edited (sgGLUT1) CAR T-cells compared to non-targeting controls (sgCtrl). Quantification of GLUT1-negative CAR T-cells is shown on the right (n = 4).

i–j, Distribution of CAR T-cell differentiation states including naïve/stem cell memory (N/SCM), central memory (CM), effector memory (EM), and effector memory RA-positive (EMRA) subsets across edited conditions (i). Frequency of $TCF1^{hi}$ CAR T cells across edited conditions (j).

k, Total protein synthesis rates (puromycin incorporation) and OXPHOS dependence of control and sgGLUT1 CAR^+ T-cells on oxidative phosphorylation, assessed by oligomycin sensitivity.

l, Extracellular acidification rate (ECAR) and glycolytic reserve measurements in control and sgGLUT1 CAR^+ T-cells.

m, Incucyte cytotoxicity assays tracking tumor cell clearance by control and sgGLUT1 CAR^+ T-cells during repetitive leukemia cell challenge. NALM6 cells were added every 48 h (arrows).

Statistical significance was determined using two-tailed paired Student's *t*-tests (h–l). *P* values are indicated as follows: $^*P < 0.05$, $^{**}P < 0.01$, $^{***}P < 0.001$, and $^{****}P < 0.0001$; ns, not significant.

Extended Data Table 1. Clinical characteristics of patients included in the CD22 CAR T-cell trial.

Patient ID	CAR construct	Diagnosis	Prior therapies*	Bone marrow disease burden†	CRS Max Grade	IEC-HS	Best overall response
1	CD22	B-cell ALL	3	3	2	No	CR (MRD-)
2	CD22	B-cell ALL	6	3	2	Yes	CR (MRD-)
3	CD22	B-cell ALL	6	3	1	No	CR (MRD-)
4	CD22	B-cell ALL	3	3	2	No	CR (MRD-)
5	CD22	B-cell ALL	6	3	0	No	SD
6	CD22	B-cell ALL	6	1	0	No	SD
7	CD22	B-cell ALL	6	2	0	No	PD
8	CD22	B-cell ALL	3	1	0	No	PD
9	CD22	B-cell ALL	2	1	0	No	PD
10	CD22	B-cell ALL	9	3	2	No	CR (MRD-)
11	CD22	B-cell ALL	6	1	3	No	CR (MRD-)
12	CD22	B-cell ALL	8	3	1	No	CR (MRD-)
13	CD22	B-cell ALL	6	3	1	No	CR (MRD-)
14	CD22	B-cell ALL	6	3	1	No	CR
15	CD22	B-cell ALL	6	3	1	No	CR (MRD-)
16	CD22	B-cell ALL	9	3	3	Yes	CR (MRD-)
17	CD22	B-cell ALL	5	1	2	No	CR (MRD-)
18	CD22	B-cell ALL	ND	ND	ND	Yes	ND
19	CD22	B-cell ALL	6	3	3	Yes	CR (MRD-)
20	CD22	B-cell ALL	3	3	2	Yes	CR (MRD-)
21	CD22	B-cell ALL	8	3	1	Yes	CR (MRD-)
22	CD22	B-cell ALL	6	3	1	No	HA
23	CD22	B-cell ALL	3	3	3	Yes	CR (MRD-)
24	CD22	B-cell ALL	5	3	2	Yes	CR (MRD-)
25	CD22	B-cell ALL	7	3	1	No	PD
26	CD22	B-cell ALL	4	3	2	Yes	PR
27	CD22	B-cell ALL	6	1	1	No	PD

***** *Number of prior therapies excluding hematopoietic stem cell transplantation*

† Bone marrow disease burden was scored on a 0–3 scale according to the clinical trial classification.

Abbreviations: B-cell ALL, B-cell acute lymphoblastic leukemia; CAR, chimeric antigen receptor; CRS, cytokine release syndrome; IEC-HS, immune effector cell-associated hemophagocytic syndrome; CR,

complete remission; MRD, minimal residual disease; PR, partial response; SD, stable disease; PD, progressive disease; HA, hematologic aplasia; ND, not determined.

Extended Data Table 2. Clinical characteristics of patients included in the CD19/CD22 CAR T-cell trials.

Patient ID	CAR construct	Diagnosis	Prior therapies*	Bone marrow disease burden†	CRS Max Grade	IEC-HS	Best overall response
1	CD19/CD22 Bivalent	B-cell ALL	8	3	3	No	CR (MRD-)
2	CD19/CD22 Bivalent	B-cell ALL	6	1	0	No	CR (MRD-)
3	CD19/CD22 Bivalent	B-cell ALL	6	1	1	No	CR (MRD-)
4	CD19/CD22 Bivalent	B-cell ALL	4	0	0	No	CR (MRD-)
5	CD19/CD22 Bicistronic	B-cell ALL	5	3	2	Yes	CR (MRD-)
6	CD19/CD22 Bicistronic	B-cell ALL	5	0	1	No	CR (MRD-)
7	CD19/CD22 Bicistronic	B-cell ALL	3	3	2	Yes	CR (MRD-)
8	CD19/CD22 Bicistronic	B-cell ALL	3	2	1	No	CR (MRD-)
9	CD19/CD22 Bicistronic	B-cell ALL	3	1	1	Yes	CR (MRD-)

***** *Number of prior therapies excluding hematopoietic stem cell transplantation*

† Bone marrow disease burden was scored on a 0–3 scale according to the clinical trial classification.

Abbreviations: B-cell ALL, B-cell acute lymphoblastic leukemia; CAR, chimeric antigen receptor; CRS, cytokine release syndrome; IEC-HS, immune effector cell-associated hemophagocytic syndrome; CR, complete remission; MRD, minimal residual disease; PR, partial response; SD, stable disease; PD, progressive disease; HA, hematologic aplasia; ND, not determined.